This paper is being published in the proceedings of the *8th AIAA/USAF/NASA/ISSMO Symposium on Multidisciplinary Analysis and Optimization*, September 6-8, 2000, Long Beach, CA, AIAA

AIAA-2000-4895

EFFICIENT PARETO FRONTIER EXPLORATION USING SURROGATE APPROXIMATIONS

Benjamin Wilson,[*] David J. Cappelleri,[†] Timothy W. Simpson,[‡] and Mary I. Frecker[§]
Department of Mechanical & Nuclear Engineering
The Pennsylvania State University
University, PA 16802

Abstract

In this paper we present an efficient and effective method of using surrogate approximations to explore the design space and capture the Pareto frontier during multiobjective optimization. The method employs design of experiments and metamodeling techniques (e.g., response surfaces and kriging models) to sample the design space, construct global approximations of the sample data, and quickly explore the design space to obtain the Pareto frontier without specifying weights for the objectives or using any optimization. To demonstrate the method, two mathematical example problems are presented. The results indicate that the proposed method is effective at capturing convex and concave Pareto frontiers even when discontinuities are present. After validating the method on the two mathematical examples, a design application involving the multiobjective optimization of a piezoelectric bimorph grasper is presented. The method facilitates the multiobjective decision making process, enabling us to find a compromise solution suitable for the given design requirements.

1. Introduction

Engineering design by its very nature is multiobjective, often requiring tradeoffs between disparate and conflicting objectives. Designing the cross-section of a cantilever beam is a classic example of the tradeoffs embodied in design—minimizing the weight and deflection of the beam requires a tradeoff between both objectives since improving one worsens the other. The pervasiveness of these tradeoffs in engineering design has given rise to a rich and vast array of methods and approaches for multiobjective and multicriteria optimization. Examples include the weighted sum and compromise programming approaches,[1-3] genetic algorithm-based approaches,[4-8] Pareto point approximation methods[9-11], and some "brute force" approaches such as Parameter Space Investigation.[12, 13]

Similarly, many researchers have studied the limitations of weighted sum approaches to capture the Pareto set in non-convex problems[14-16]. Messac, et al.[16] derive quantitative conditions for determining whether or not a Pareto point is capable of being captured with a given objective function formulation. Das and Dennis[17] also examine the drawbacks of using weighted sums to find the Pareto set during multicriteria optimization, noting that an evenly distributed set of weights fails to produce an even distribution of points in the Pareto set. Their observations led to the development of the Normal-Boundary Intersection (NBI) method to parameterize the Pareto set and generate an evenly distributed set of points in the Pareto set using an evenly distributed set of parameters.[18-20]

Balling[21] likens multiobjective optimization to "shopping" in that the goal as designers should be to produce a "rich set of good designs" from which the consumer can pick the best design. He advocates the need for research in two areas: (1) efficient methods for obtaining rich Pareto sets and (2) interactive graphical computer tools to assist decision-makers in the "shopping" process. Balling and his colleagues have developed an approach that combines genetic algorithms to find Pareto optimal designs with an interactive GUI that has slider bars to vary the importance of the objectives to determine their impact on the design solution. Tappeta and Renaud[22,23] are also developing an interactive multiobjective optimization procedure to explore design solutions around a Pareto point using second-order Pareto surface approximations derived from sensitivity information at the Pareto point. Implementation of their approach using the Physical Programming methodology is described in Ref. 24.

---

[*] Graduate Research Assistant.
[†] Graduate Research Assistant.
[‡] Assistant Professor and AIAA Member. Please email correspondences to tws8@psu.edu.
[§] Assistant Professor.

In this paper, we *seek to reduce the computational expense of interactive approaches to multiobjective optimization by focusing on efficient methods for obtaining rich Pareto sets.* Consequently, we propose a method that employs design of experiments (e.g., central composite designs, orthogonal arrays, and latin hypercubes) and surrogate approximations (e.g., response surfaces and kriging models) to facilitate exploring and capturing the Pareto frontier. Our method for efficient Pareto frontier exploration is introduced in the next section. This is followed in Sections 3 and 4 with two example problems used to illustrate the capability of the proposed Pareto frontier exploration method to function effectively for convex and non-convex multicriteria optimization problems even when discontinuities are present. Following these test problems, Section 5 contains an application of multiobjective optimization to design a piezoelectric bimorph actuator for use in minimally invasive surgery. Closing remarks are given in Section 6.

2. Technology Base

In this work, we do not seek to approximate the Pareto frontier directly as previous researchers have, nor do we require that any weights for the objectives be specified *a priori* for a weighted sum or compromise programming approach. Instead, we propose a method to explore the entire design space rapidly by combining design of experiments (e.g., central composite designs, OAs, and latin hypercubes) and metamodeling techniques (e.g., response surfaces and kriging models) to construct inexpensive-to-run approximations of computationally expensive engineering analyses and simulations.[25] These "surrogate" approximations are then used in lieu of the computationally expensive analyses to explore the multiobjective design space and identify a rich set of potential points along the Pareto frontier. Candidate points can then be used to obtain the actual (or near actual) Pareto frontier from the original analysis codes after good designs are identified for the multiple competing objectives.

2.1 The Pareto Frontier Exploration Method

Our proposed method for Pareto frontier exploration is shown in Figure 1. As seen in the figure, the proposed approach employs design of experiments and surrogate approximations to facilitate exploring and capturing the Pareto frontier. As shown in Figure 1, the first step is to identify the design space. This is typically a multi-dimensional hypercube defined by the upper and lower bounds of each design variable over some region of interest. Once the design space has been identified, an experimental design is selected to sample the design space. A variety of different types of experimental designs exist, including central composite designs,[26] Latin hypercubes,[27] and orthogonal arrays[28] to name a few. After choosing an experimental design, the design space is sampled to obtain data to construct surrogate approximations of each objective and constraint.

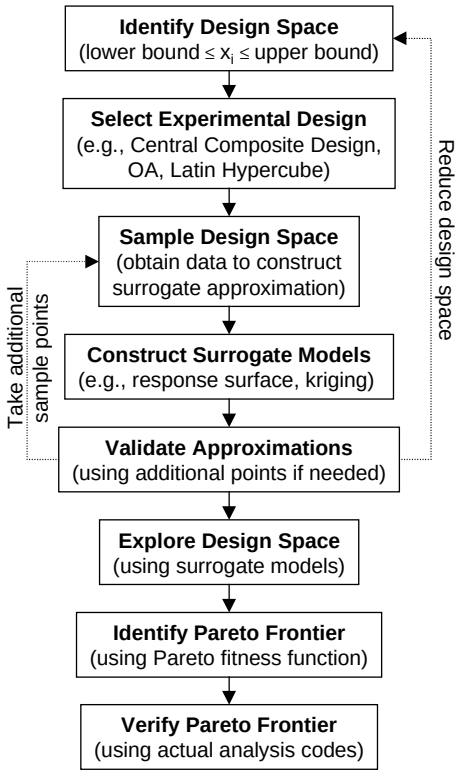

Figure 1 Pareto Frontier Exploration Method

Once the sample data has been obtained, the next step is to construct surrogate approximations. In this paper, we demonstrate the method using two types of surrogate models: (1) second-order polynomial response surfaces[26] and (2) kriging models which employ an underlying constant term and a Gaussian correlation function (see Refs. 29-33 for a detailed description of kriging and example applications). A variety of surrogate approximations exist, however, and choosing the appropriate approximation is an open research question receiving considerable attention. Recent reviews of surrogate modeling applications in mechanical and aerospace engineering are given in Ref. 34, structural optimization in Ref. 35, and multidisciplinary design optimization in Ref. 36.

After the approximations have been constructed, they must be validated to ensure sufficient accuracy. Validation can be achieved through a variety of means, including residual error analysis, R^2 computation, and cross-validation. In the case of kriging models, additional validation points are often required since a kriging model interpolates the sample data. The additional validation data is then used to compute error measures—where error is defined as the difference

between the predicted and actual values—such as mean absolute error (MAE), average absolute error (AAE), and root mean squared error (RMSE) over the additional validation data. If the errors are too large, additional sample points may be taken or the design space may be reduced in an effort to improve the accuracy of the approximation. If the approximations are not sufficiently accurate, then the Pareto frontier obtained using the surrogate approximations will not be a good approximation of the actual Pareto frontier. In the examples in Sections 3-4, a comparison of the predicted and actual Pareto frontiers is used to validate the approximations; additional validation data is used in Section 5 to help validate the surrogate approximations.

Once the surrogate models have been validated, they can be used to explore the design space using an exhaustive grid search. Since the approximations are simple, they are extremely fast to execute; therefore, an exhaustive grid search over the design space is relatively inexpensive. After the design space has been explored over the search grid, the Pareto frontier can be obtained using a Pareto fitness function such as that proposed in Ref. 8:

$$F_i = [1 - \max_{j \neq i}(\min(f1_i - f1_j, f2_i - f2_j, ...))]^p \quad (1)$$

where:

F_i = Pareto fitness value of ith design
$f1_i$ = first objective function value of the ith design
$f2_i$ = second objective function value of the ith design
p = pareto exponent (p = 1 in this study)

Using Eqn. 1, Pareto optimal designs have a fitness function value greater than or equal to one; non-Pareto designs have fitness values between 0 and 1. This occurs because the objectives f1, f2, etc. in Eqn. 1 are scaled to range between zero and one using the following equation:

$$f1_i = \frac{rawf1_i - rawf1_{\min}}{rawf1_{\max} - rawf1_{\min}} \quad (2)$$

where:

$f1_i$ = scaled first objective value
$rawf1_i$ = raw (unscaled) value of first objective for ith design
$rawf1_{max}$ = maximum raw (unscaled) value of first objective over all designs
$rawf1_{min}$ = minimum raw (unscaled) value of first objective over all designs

This scaling assumes that all objectives are to be minimized; however, the scaling can be easily reversed to maximize objectives if needed.

This "brute force" approach enables us to capture the entire Pareto frontier all at once without having to specify weights on the objectives or utilize any optimization algorithm. The predicted Pareto frontier can then be explored graphically to determine suitable design solutions that yield the best compromise between the multiple objectives. The corresponding design variables can be stored along with the Pareto points, enabling the actual Pareto frontier to be easily constructed from the original analysis code by substituting these design variables into the original analyses rather than the surrogate approximation.

The proposed approach does not restrict the use of an optimization algorithm to facilitate the search for the Pareto frontier using the surrogate approximations; however, we do wish to avoid having to specify weights *a priori* for each objective. We envision that a genetic algorithm-based approach such as that proposed in Refs. 4, 5, and 8 could greatly facilitate the design space search, particularly in large dimensions; however, we do not implement such an approach in this paper since our problem sizes do not warrant it.

2.2 Surrogate Modeling Software

To facilitate construction and validation of the surrogate approximations, a platform-independent Java-based software application has been developed. After initialization (see Figure 2), the surrogate modeling application queries the user for the design variables and their ranges of interest and the output responses (see Figure 3). The user then selects an experimental design, and a set of data points are generated and sent to the analysis code or simulation (see Figure 4). The application then constructs the selected surrogate approximation using the resulting sample data (see Figure 5) and outputs a separate Java class file, containing the corresponding surrogate model. This Java class can then be compiled and queried as needed in place of the original analysis code. The validation tab (not shown) is currently under development.

Figure 2 Surrogate Modeler – Initialization Tab

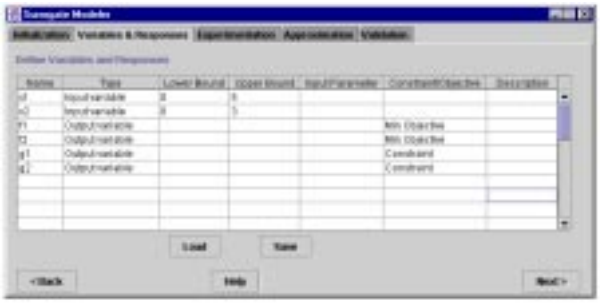

Figure 3 Surrogate Modeler – Variables & Responses Tab

Figure 4 Surrogate Modeler – Experimentation Tab

Figure 5 Surrogate Modeler – Approximation Tab

To demonstrate the utility of surrogate approximations and the effectiveness of the proposed method for capturing the Pareto frontier, two mathematical example problems are presented next.

3. Example Problem #1

The first example is a convex, bi-criteria mathematical function with linear boundary constraints from Ref. 10. This example is formulated as follows.

Minimize: $f_1(x_1, x_2) = (x_1 - 2)^2 + (x_2 - 1)^2$
$f_2(x_1, x_2) = x_1^2 + (x_2 - 6)^2$

subject to: $g_1(x_1, x_2) = x_1 - 1.6 \le 0$
$g_2(x_1, x_2) = 0.4 - x_1 \le 0$
$g_3(x_1, x_2) = x_2 - 5 \le 0$
$g_4(x_1, x_2) = 2 - x_2 \le 0$

Since the four linear constraints, *g1-g4*, specify the region of interest ($x_1 \in [0.4, 1.6]$ and $x_2 \in [2, 5]$), we choose to sample only within this region to avoid infeasible solutions. Therefore, the only surrogate approximations that need to be constructed in this example are for *f1* and *f2*, not the constraints.

Two experimental designs are used to sample the design space as shown in Figure 6: a central-composite design (CCD) and a Latin hypercube (LH). Both designs contain nine points to ensure a fair comparison between the resulting approximations.

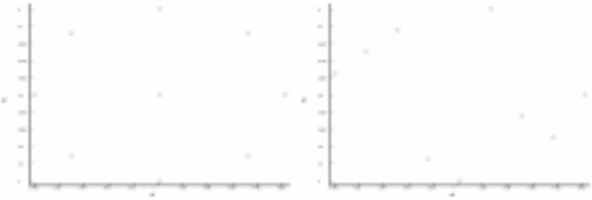

(a) 9 point CCD **(b) 9 point LH**

Figure 6 Experimental Designs for Examples 1 & 2

The actual values of *f1* and *f2* at each sample point are recorded, and the resulting set of sample data is used to construct second-order response surface models and kriging models for each objective for each sample set. These surrogate models are then used to predict the responses at a set of new design points; we sample a 101 x 101 grid of points to generate the Pareto frontier using the Pareto fitness function given in Eqn. 1. The resulting Pareto frontiers obtained using the response surface models and the kriging models are shown in Figure 7 and Figure 8, respectively. Since this example consists of two convex, second-order polynomial functions, the full quadratic response surface predicts the new points exactly, for both experimental designs. Consequently, the predicted and actual Pareto frontiers are identical for the response surface models.

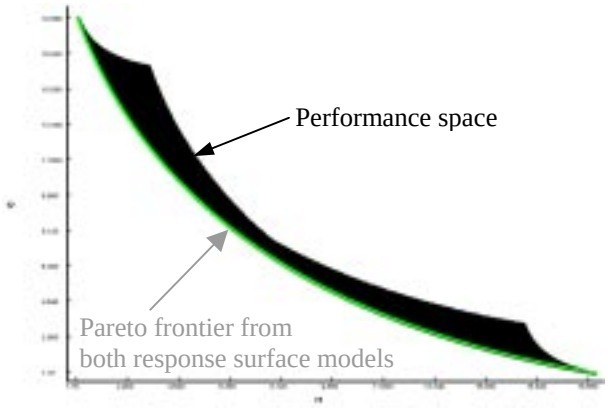

Figure 7 Response Surface Pareto Frontier

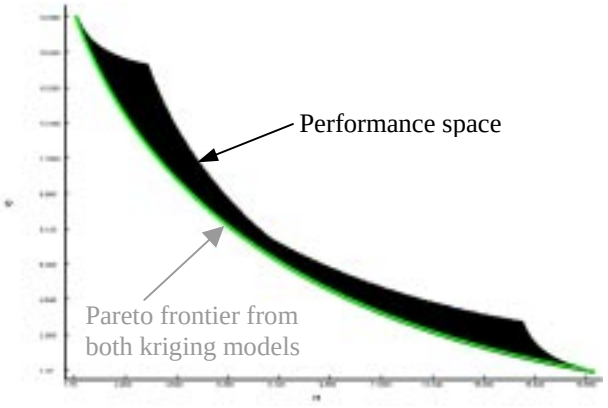

Figure 8 Kriging Pareto Frontier

While the response surfaces fit *f1* and *f2* exactly, error analysis using maximum absolute error (MAE), average absolute error (AAE), and root mean square error (RMSE), is performed on the kriging model for validation of the Pareto frontier predictions. The results of this analysis are listed in Table 1 and are obtained by comparing the values of *f1* and *f2* along the actual Pareto frontier with the corresponding predicted values of *f1* and *f2* based on the kriging approximations.

Table 1 Validation of Kriging Pareto Frontiers

Error Measure	*Kriging with Central Composite Design*		*Kriging with Latin Hypercube*	
	f1	**f2**	**f1**	**f2**
MAE	0.2632	0.0811	0.0064	0.0047
AAE	0.2587	0.0776	0.0007	0.0008
RMSE	0.2587	0.0776	0.0013	0.0010

Note that the errors listed in Table 1 are quite small compared to the actual values of *f1* and *f2*, indicating that the kriging models—using only a constant term and a Gaussian correlation function—are nearly as accurate as a full second-order polynomial response surface. Also note that the kriging models based on the Latin hypercubes are much more accurate than those based on the central composite design. This trend is investigated further in our second example in the next section.

4. Example Problem #2

Our second example is a two-dimensional problem with non-linear objectives and constraints from Ref. 22. The problem definition is as follow.

$$\text{Minimize: } f_1(x_1, x_2) = (x_1 + x_2 - 7.5)^2 + (x_2 - x_1 + 3)^2/4$$
$$f_2(x_1, x_2) = (x_1 - 1)^2/4 + (x_2 - 4)^2/2$$

$$\text{subject to: } g_1(x_1, x_2) = 2.5 - (x_1 - 2)^3/2 - x_2 \geq 0$$
$$g_2(x_1, x_2) = 3.85 + 8(x_2 - x1 + 0.65)^2 - x_2 - x_1 \geq 0$$

The bounds $0 \leq x_1 \leq 5$ and $0 \leq x_2 \leq 3$ are used to ensure that the entire feasible performance space is utilized. Response surface and kriging models are created for the second example problem, using the same nine point Latin hypercube and central-composite design shown previously in Figure 6. Once again, the response surface models, for both experimental designs, predict the Pareto frontier exactly as shown in Figure 9. The Pareto frontiers obtained from the kriging models from both experimental designs are shown in Figure 10.

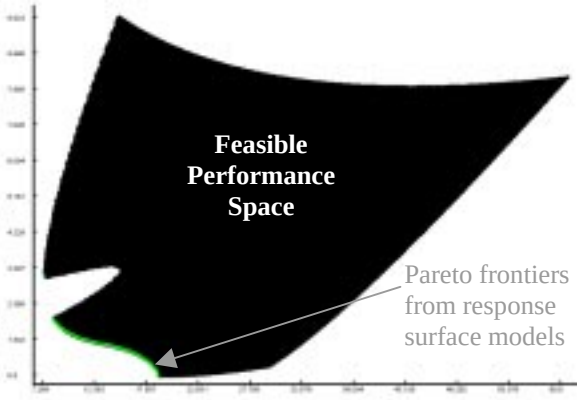

Figure 9 Response Surface Pareto Frontier

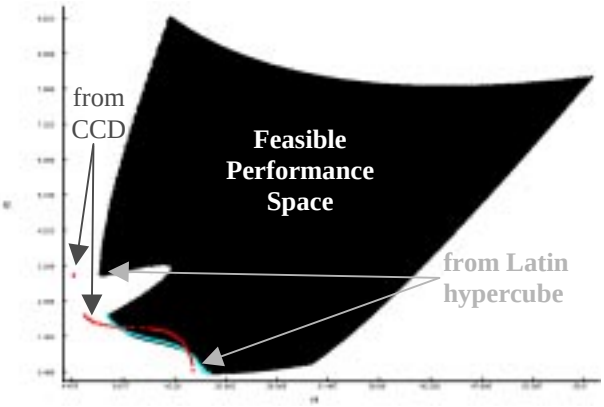

Figure 10 Kriging Pareto Frontier for CCD and Latin Hypercube Designs

As seen in Figure 10, the kriging models created using the Latin hypercube design accurately predicts the Pareto frontier, but the kriging models created using the central composite design do not. Error measurements for *f1* and *f2* for the points along the Pareto frontier for both sets of kriging models are listed in Table 2.

Table 2 Validation of Kriging Pareto Frontiers

Error Measure	*Kriging with Central Composite Design*		*Kriging with Latin Hypercube*	
	f1	**f2**	**f1**	**f2**
MAE	2.0808	0.2565	0.0094	0.2708
AAE	2.0615	0.2579	0.0074	0.2460
RMSE	2.0616	0.3306	0.0076	0.2986

Based on this data, we note that the kriging models based on the central composite design are much less accurate than those obtained using the Latin hypercube design. The discrepancy results from an interaction between the kriging model and the experimental design type. Due to the location and spacing of the sample points in the design space in a central composite design, the correlation matrix based on the Gaussian correlation function in the fitted kriging model tends to be singular or near singular when maximum likelihood estimation is performed to obtain the theta parameters used to fit the model. To confirm this, the condition numbers of the correlation matrices for each response for each design are listed in Table 3. We have found that a condition number smaller than 10^{-12} indicates that significant round-off error can occur during prediction because the correlation matrix is close to singular. Such is the case for the kriging models of *f1* and *f2* based on the central composite design.

Table 3 Condition Numbers of Kriging Model Correlation Matrices

Condition Number	*Kriging with Central Composite Design*	*Kriging with Latin Hypercube*
f1	2.8821D-15	1.2165D-09
f2	1.3950D-14	8.5201D-10
g1	1.0345D-08	2.2178D-09
g2	6.4121D-13	2.2982D-06

Despite the slight approximation error in the kriging models, the Pareto points themselves (i.e., the design variables x_1 and x_2 corresponding to each point on the Pareto frontier) are nearly identical to the actual Pareto points obtained from the original set of equations, see Figure 11 and Figure 12. Figure 11 shows the Pareto points obtained from the response surface models overlaying the actual Pareto points; those obtained from the kriging models based on the Latin hypercube design are shown in Figure 12.

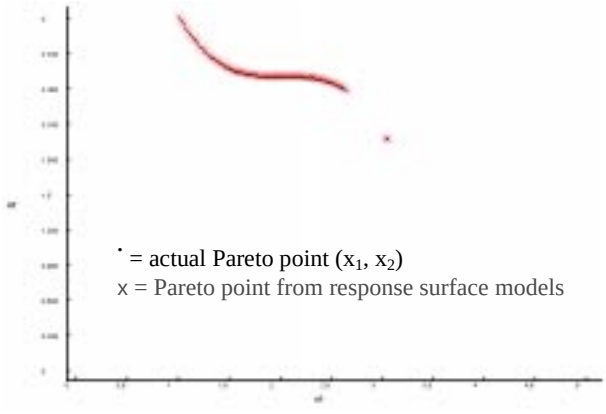

Figure 11 Pareto Frontier Points for Response Surface Models for Example 2

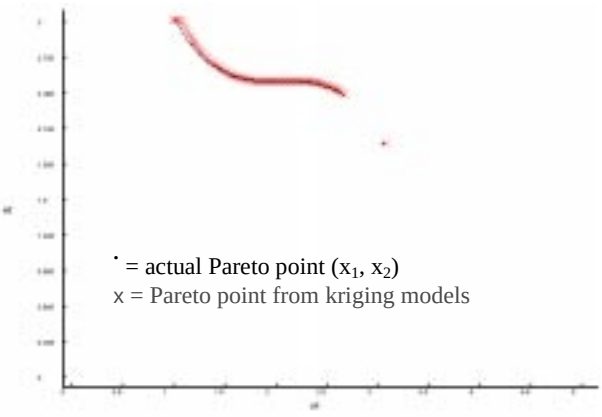

Figure 12 Pareto Frontier Points for Kriging Models for Example 2

While considerable error exists in the Pareto frontier obtained using the kriging models based on the central composite design, the kriging models based on the Latin hypercube design and both sets of response surface models are able to capture the Pareto frontier accurately. In this case, the Pareto frontier is successfully captured without the use of optimization even though it is non-convex and discontinuous. Furthermore, this also demonstrates the importance of validating the surrogate approximations to ensure that they are sufficiently accurate before attempting to capture the Pareto frontier; otherwise, the predicted frontier and the actual frontier may be vastly different.

5. Design of a Piezoelectric Bimorph Actuator

Our final example comes from current research work in which we are trying to simultaneously optimize the maximum deflection and blocked force of a piezoelectric bimorph actuator for minimally invasive surgery.[37-39] A piezoelectric bimorph actuator is created by laminating layers of piezoelectric ceramic material (PZT) onto a thin sandwich beam or plate. When opposing voltages are applied to the two ceramic layers, a bending moment is induced in the beam, see Figure 13. A pair of cantilevered piezoelectric bimorph actuators can be used as a simple grasping device, where the bimorph actuators are used as active "fingers" as shown in Figure 14.

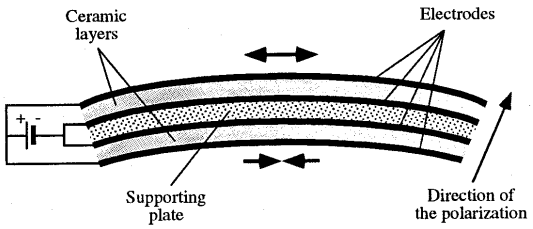

Figure 13 A Piezoelectric Bimorph[40]

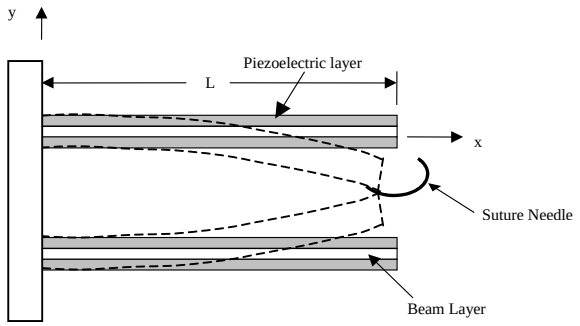

Figure 14 A Piezoelectric Bimorph Grasper

The objective in this example is to design a PZT bimorph grasper for application in minimally invasive surgical procedures. The performance of the PZT bimorph actuator is evaluated in terms of the tip force and deflection; a large tip deflection is required so that the jaws of the grasper can close completely, and a large tip force is required to securely grasp a suture needle and prevent it from rolling in the jaws. These performance criteria are determined by the thickness and width of each PZT layer, the length of the actuator, the material properties, and the applied voltage. The force available at the tip is modeled as the blocked force (i.e., the force exerted with no deflection), and the deflection is modeled as the free deflection. The results from preliminary analysis indicate that a standard, commercially available bimorph is infeasible for MIS applications since there is insufficient grasping force and tip deflection.[39] Consequently, a variable thickness design, where the thickness of the layers is varied along the length, is proposed to improve the deflection and force performance of the PZT bimorph actuator.

The piezoelectric bimorph actuator is modeled as a composite beam with a thin steel sandwich layer and PZT5H top and bottom layers. Rather than allowing the thickness of the PZT layers to vary continuously along the length, the layers are discretized into five sections to allow for simple modeling, where the thickness of each section, t_i (i=1,…,5), are the design variables (see Figure 15). A finite element model of the composite variable thickness design is created with standard cantilever supports at the base nodes. The finite element model consists of 1458 eight-node three-dimensional (brick) elements as shown in Figure 16. Each PZT section has three elements across its height and width, and 10 elements along the length. As the thickness of the PZT sections is varied in the optimization procedure, the number of elements remains constant. Node compatibility at the section boundaries is ensured through the use of transition elements as shown in Figure 15. These elements are formed by joining the end nodes from one piezoelectric section to the start nodes of the next piezoelectric section. The length of the transition elements, x_{tr}, is constant. The steel beam is modeled using 486 brick elements, with each section having three elements along the height and width and ten across the length.

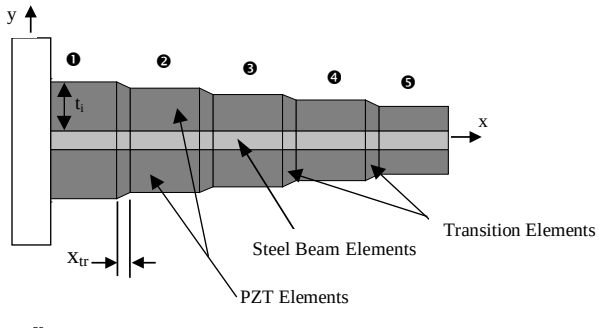

Figure 15 Variable Thickness Actuator

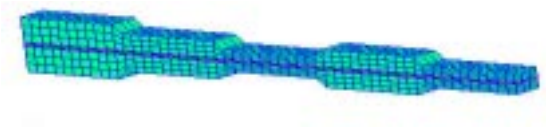

Figure 16 Finite Element Model of Actuator

The finite element analysis is performed using ABAQUS. Two types of FE analysis are conducted to predict (1) the free deflection of the bimorph and (2) the blocked force while the actuator is subjected to a prescribed input voltage. The blocked force condition is simulated by constraining the nodes at the tip of the bimorph in the y-direction. Since the operating frequency is low (on the order of 1-2 Hz) in MIS applications, only quasi-static response is considered.

A twenty-seven point central composite face-centered design is used to sample the design space of interest defined by the lower and upper bounds of the five thickness variables ($1 \text{ mm} \le t_i \le 3 \text{ mm}$, i = 1, …, 5). Data is generated from these 27 sample points to construct two sets of approximations for comparison: (1) response surface models and (2) kriging approximations for both blocked force and deflection. Both sets of approximations are then used in lieu of the ABAQUS finite element simulation to search the design space to find the approximate Pareto frontier.

After constructing both sets of approximations, a set of twenty-five random points from a Latin hypercube are used to validate each set of surrogate approximations. A summary of the maximum absolute % error, average absolute % error, and root mean square error (RMSE) for the response surface and kriging models for the deflection and blocked force responses is given in Table 4. The error in the predicted deflection is comparable

for both approximations, with the response surface model having slightly lower maximum and average percent error. However, in the case of the blocked force response, the kriging model fits the data much more accurately. Based on the RMSE for the predicted deflection and blocked force, the kriging model is more accurate than the response surface model.

Table 4 Validation of Surrogate Approximations

Error Measure	*Response Surface*		*Kriging Model*	
	Deflection	**Force**	**Deflection**	**Force**
MAE(%)	13.78	18.99	18.06	8.02
AAE(%)	6.23	4.33	7.09	2.83
RMSE	1.08E-03	1.47E-02	1.20E-06	8.35E-05

To understand the tradeoff between the deflection and blocked force objectives, the approximations are used to search the design space and find the Pareto frontier. The design space is explored by predicting the blocked force and deflection of 3125 design points (from a 5^5 grid) using the response surface models and the kriging models. The Pareto frontier is then obtained by selecting points on the boundary of the design space as predicted by the response surface models and the kriging models as shown in Figure 17. The points on the Pareto frontier, as predicted by the response surface models and kriging models, are compared to one another, and the points with common thickness settings are evaluated in ABAQUS to verify the actual response. The results of this analysis are also shown in Figure 17. As seen in the figure, the kriging models are good predictors of the points along the Pareto frontier, while the response surface models are not for points that have a large deflection and small blocked force. This result is consistent with the data in Table 4 as the response surface model is generally less accurate than the kriging model based on the set of validation points. It is also evident from Figure 17 that by varying the thickness of the piezoelectric layers a substantial blocked force can be generated, but the tip deflection is still quite low.

To examine the inadequacies of the weighted sum approach typically used in multiobjective optimization, a final study is conducted to determine the impact of the value of the weighting factor *w* on the optimal solution of the weighted sum of both objectives (i.e., maximize deflection and blocked force):

$$f = (1-w)\frac{\delta^*_{free} - \delta_{free}}{\delta^*_{free}} + (w)\frac{F^*_{blocked} - F_{blocked}}{F^*_{blocked}} \qquad (3)$$

where δ^*_{free} and $F^*_{blocked}$ are the individual optimum values of free deflection and blocked force, respectively. The weighting factor, *w*, is varied from 0.0 to 1.0, using increments of 0.01. Table 5 and Table 6 show the effect of the weighting factor on the optimal solutions for the response surface and kriging models, respectively. Although we expect to obtain several intermediate solutions by varying the weighting factor, only the two extreme solutions and one intermediate solution are obtained using the response surface models. As the weight on the deflection is increased, the maximum deflection solution is obtained until the weighting factor reaches 0.59, after which an intermediate solution is obtained until w= 0.88. The maximum force solution is obtained when the weighting factor is in the range 0.89-1.00. Using the kriging model, three intermediate solutions are obtained during optimization. This confirms the inadequacy of using the weighted sum approach to capture the Pareto frontier for non-convex problems; the proposed surrogate modeling based approach is much more efficient at capturing the entire Pareto frontier without having to specify weights for the objectives or use an optimization algorithm.

6. Closing Remarks

Preliminary results indicate that the surrogate approximations prove to be a useful means for quickly and effectively visualizing the relationship between competing objectives and can be used to explore the design space quickly to capture the Pareto frontier. The Pareto frontier in Sections 3 and 4 is obtained using a Pareto fitness function, Eqn. 1, without the need to specify weights for the objective functions or enlist the aid of optimization. The approach works well for both convex and non-convex Pareto frontiers, even when discontinuities are present; however, the importance of validation cannot be stressed enough as discussed in Section 4. Finally, flexibility of the proposed approach has been demonstrated by using two types of experimental designs (i.e., central composite designs and Latin hypercubes) and two types of surrogate approximations (i.e., response surfaces and kriging models). The method can easily accommodate a wide variety of experimental designs and approximations.

While three examples does not completely validate the method, the results to date are promising. Additional testing of the proposed approach on a variety of convex and non-convex multiobjective optimization problems continues. While the examples contained herein are for multicriteria problems with two objectives, we do not anticipate any problems scaling our approach to multicriteria problems with more than two objectives. We are currently seeking additional examples to validate these claims and continue testing the method.

Acknowledgements

The work by Ben Wilson and Dr. Simpson is supported by Dr. Kam Ng, ONR 333, through the Naval Sea Systems Command under Contract No. N00039-97-D-0042 and N00014-00-G-0058. The work by Dave Cappelleri and Dr. Frecker is supported by the Charles E. Culpeper Foundation Biomedical Pilot Initiative.

References

[1] Osyczka, A., "Multicriteria Optimization for Engineering Design," *Design Optimization (Gero, J. S., ed.)*, Academic Press, New York, 1985, pp. 193-227.

[2] Stadler, W. and Dauer, J., "Multicriteria Optimization in Engineering: A Tutorial and Survey," *Structural Optimization: Status and Promise (Kamat, M. P., ed.)*, AIAA, Washington, D.C., 1993, pp. 209-249.

[3] Steuer, R. E., *Multiple Criteria Optimization: Theory, Computation, and Application*, Wiley, New York, 1986.

[4] Azarm, S., Reynolds, B. J. and Narajanan, S., "Comparison of Two Multiobjective Optimization Techniques with and within Genetic Algorithms," *Advances in Design Automation*, Las Vegas, NV, ASME, September 12-15, 1999, Paper No. DETC99/DAC-8584.

[5] Balling, R. J., Taber, J. T., Brown, M. R. and Day, K., "Multiobjective Urban Planning Using Genetic Algorithm," *Journal of Urban Planning and Development*, Vol. 125, No. 2, 1999, pp. 86-99.

[6] Cheng, F. Y. and Li, D., "Multiobjective Optimization Design with Pareto Genetic Algorithm," *Journal of Structural Engineering*, Vol. 123, No. 9, 1997, pp. 1252-1261.

[7] Osyczka, A. and Kundu, S., "A New Method to Solve Generalized Multicriteria Optimization Problems Using the Simple Genetic Alrogithm," *Structural Optimization*, Vol. 10, No. 2, 1995, pp. 94-99.

[8] Schaumann, E. J., Balling, R. J. and Day, K., "Genetic Algorithms with Multiple Objectives," *7th AIAA/USAF/NASA/ISSMO Symposium on Multidisciplinary Analysis & Optimization*, St. Louis, MO, AIAA, Vol. 3, September 2-4, 1998, pp. 2114-2123. AIAA-98-4974.

[9] Kasprazak, E. M. and Lewis, K. E., "A Method to Determine Optimal Relative Weights for Pareto Solution Sets," *Proceedings of the Third World Congress of Structural and Multidisciplinary Optimization (WCSMO-3) (Bloebaum, C. L., Lewis, K. E., et al., eds.)*, Buffalo, NY, University at Buffalo, Vol. 2, May 17-21, 1999, pp. 408-410.

[10] Li, Y., Fadel, G. M. and Wiecek, M. M., "Approximating Pareto Curves Using the Hyper-Ellipse," *7th AIAA/USAF/NASA/ISSMO Symposium on Multidisciplinary Analysis & Optimization*, St. Louis, MO, AIAA, Vol. 3, September 2-4, 1998, pp. 1990-2002.

[11] Zhang, J., Wiecek, M. M. and Chen, W., "Local Approximation of the Efficient Frontier in Robust Design," *Advances in Design Automation*, Las Vegas, NV, ASME, September 12-15, 1999, Paper No. DETC99/DAC-8566.

[12] Liberman, E. R., "Soviet Multi-Objective Mathematical Programming Methods: An Overview," *Management Science*, Vol. 37, No. 9, 1991, pp. 1147-1165.

[13] Sobol, I. M., "An Efficient Approach to Multicriteria Optimum Design Problems," *Surveys on Mathematics for Industry*, Vol. 1, 1992, pp. 259-281.

[14] Athan, T. W. and Papalambros, P. Y., "A Note on Weighted Criteria Methods for Compromise Solutions in Multi-Objective Optimization," *Engineering Optimization*, Vol. 27, No. 2, 1996, pp. 155-176.

[15] Koski, J., "Defectiveness of Weighting Method in Multicriterion Optimization of Structures," *Communications in Applied Numerical Methods*, Vol. 1, No. 6, 1985, pp. 333-337.

[16] Messac, A., Sundararaj, J. G., Tappeta, R. V. and Renaud, J. E., "The Ability of Objective Functions to Generate Non-Convex Pareto Frontiers," *40th AIAA/ASME/ASCE/AHS/ASC Structures, Structural Dynamics, and Materials Conference and Exhibit*, St. Louis, MO, AIAA, Vol. 1, April 12-15, 1999, pp. 78-87. AIAA-99-1211.

[17] Das, I. and Dennis, J. E., "A Closer Look at Drawbacks of Minimizing Weighted Sums of Objectives for Pareto Set Generation in Multicriteria Optimization Problems," *Structural Optimization*, Vol. 14, No. 1, 1997, pp. 63-69.

[18] Das, I., "Optimization Large Systems via Optimal Multicriteria Component Assembly," *7th AIAA/USAF/NASA/ISSMO Symposium on Multidisciplinary Analysis & Optimization*, St. Louis, MO, AIAA, Vol. 1, September 2-4, 1998, pp. 661-669. AIAA-98-4791.

[19] Das, I., "An Improved Technique for Choosing Parameters for Pareto Surface Generation Using Normal-Boundary Intersection," *Proceedings of the Third World Congress of Structural and Multidisciplinary Optimization (WCSMO-3) (Bloebaum, C. L., Lewis, K. E., et al., eds.)*, Buffalo, NY, University at Buffalo, Vol. 2, May 17-21, 1999, pp. 411-413.

[20] Das, I. and Dennis, J. E., "Normal-Boundary Intersection: A New Method for Generating the Pareto Surface in Nonlinear Multicriteria Optimization Problems," *SIAM Journal on Optimization*, Vol. 8, No. 3, 1998, pp. 631-657.

[21] Balling, R., "Design by Shopping: A New Paradigm?," *Proceedings of the Third World Congress of Structural and Multidisciplinary Optimization (WCSMO-3) (Bloebaum, C. L., Lewis, K. E., et al., eds.)*, Buffalo, NY, University at Buffalo, Vol. 1, May 17-21, 1999, pp. 295-297.

[22] Tappeta, R. V. and Renaud, J. E., "Interactive Multiobjective Optimization Design Strategy for Decision Based Design," *Advances in Design Automation*, Las Vegas, NV, ASME, September 12-15, 1999, Paper No. DETC99/DAC-8581.

[23] Tappeta, R. V. and Renaud, J. E., "Interactive Multiobjective Optimization Procedure," *40th AIAA/ASME/ASCE/AHS/ASC Structures, Structural Dynamics, and Materials Conference and Exhibit*, St. Louis, MO, AIAA, Vol. 1, April 12-15, 1999, pp. 27-41. AIAA-99-1207.

[24] Tappeta, R. V., Renaud, J. E., Messac, A. and Sundararaj, J. G., "Interactive Physical Programming: Tradeoff Analysis and Decision Making in Multicriteria Optimization," *40th AIAA/ASME/ASCE/AHS/ASC Structures, Structural Dynamics, and Materials Conference and Exhibit*, St. Louis, MO, AIAA, Vol. 1, April 12-15, 1999, pp. 53-67. AIAA-99-1209.

[25] Simpson, T. W., Mauery, T. M., Korte, J. J. and Mistree, F., "Kriging Metamodels for Global Approximation in Simulation-Based Multidisciplinary Design Optimization," *AIAA Journal*, 2000, under review.

[26] Myers, R. H. and Montgomery, D. C., *Response Surface Methodology: Process and Product Optimization Using Designed Experiments*, John Wiley & Sons, New York, 1995.

[27] McKay, M. D., Beckman, R. J. and Conover, W. J., "A Comparison of Three Methods for Selecting Values of Input Variables in the Analysis of Output from a Computer Code," *Technometrics*, Vol. 21, No. 2, 1979, pp. 239-245.

[28] Owen, A. B., "Orthogonal Arrays for Computer Experiments, Integration and Visualization," *Statistica Sinica*, Vol. 2, 1992, pp. 439-452.

[29] Booker, A. J., "Design and Analysis of Computer Experiments," *7th AIAA/USAF/NASA/ISSMO Symposium on Multidisciplinary Analysis & Optimization*, St. Louis, MO, AIAA, Vol. 1, September 2-4, 1998, pp. 118-128. AIAA-98-4757.

[30] Giunta, A., Watson, L. T. and Koehler, J., "A Comparison of Approximation Modeling Techniques: Polynomial Versus Interpolating Models," *7th AIAA/USAF/NASA/ISSMO Symposium on Multidisciplinary Analysis & Optimization*, St. Louis, MO, AIAA, Vol. 1, September 2-4, 1998, pp. 392-404. AIAA-98-4758.

[31] Koehler, J. R. and Owen, A. B., "Computer Experiments," *Handbook of Statistics (Ghosh, S. and Rao, C. R., eds.)*, Elsevier Science, New York, 1996, pp. 261-308.

[32] Sacks, J., Welch, W. J., Mitchell, T. J. and Wynn, H. P., "Design and Analysis of Computer Experiments," *Statistical Science*, Vol. 4, No. 4, 1989, pp. 409-435.

[33] Simpson, T. W., Mauery, T. M., Korte, J. J. and Mistree, F., "Comparison of Response Surface and Kriging Models for Multidisciplinary Design Optimization," *7th AIAA/USAF/NASA/ISSMO Symposium on Multidisciplinary Analysis & Optimization*, St. Louis, MO, AIAA, Vol. 1, September 2-4, 1998, pp. 381-391. AIAA-98-4755.

[34] Simpson, T. W., Peplinski, J., Koch, P. N. and Allen, J. K., "Metamodels for Computer-Based Engineering Design: Survey and Recommendations," *Engineering with Computers*, 2000, pp. under review.

[35] Barthelemy, J.-F. M. and Haftka, R. T., "Approximation Concepts for Optimum Structural Design - A Review," *Structural Optimization*, Vol. 5, 1993, pp. 129-144.

[36] Sobieszczanski-Sobieski, J. and Haftka, R. T., "Multidisciplinary Aerospace Design Optimization: Survey of Recent Developments," *Structural Optimization*, Vol. 14, 1997, pp. 1-23.

[37] Cappelleri, D. J. and Frecker, M. I., "Optimal Design of Smart Tools for Minimally Invasive Surgery," *Optimization in Industry II (Mistree, F. and Belegundu, A. D., eds.)*, Banff, Alberta, Canada, ASME, July 6-11, 1999.

[38] Cappelleri, D. J., Frecker, M. I. and Simpson, T. W., "Optimal Design of a PZT Bimorph Actuator for Minimally Invasive Surgery," *7th International Symposium on Smart Structures and Materials*, Newport Beach, CA, SPIE, March 5-9, 1999, pp. accepted for publication.

[39] Cappelleri, D. J., Frecker, M. I., Simpson, T. W. and Snyder, A., "A Metamodel-Based Approach for Optimal Design of a PZT Bimorph Actuator for Minimally Invasive Surgery," *Journal of Mechanical Design*, 2000, under review.

[40] Fatikow, W. and Rembold, U., *Microsystem Technology and Microrobotics*, Springer-Verlag, New York, 1997.

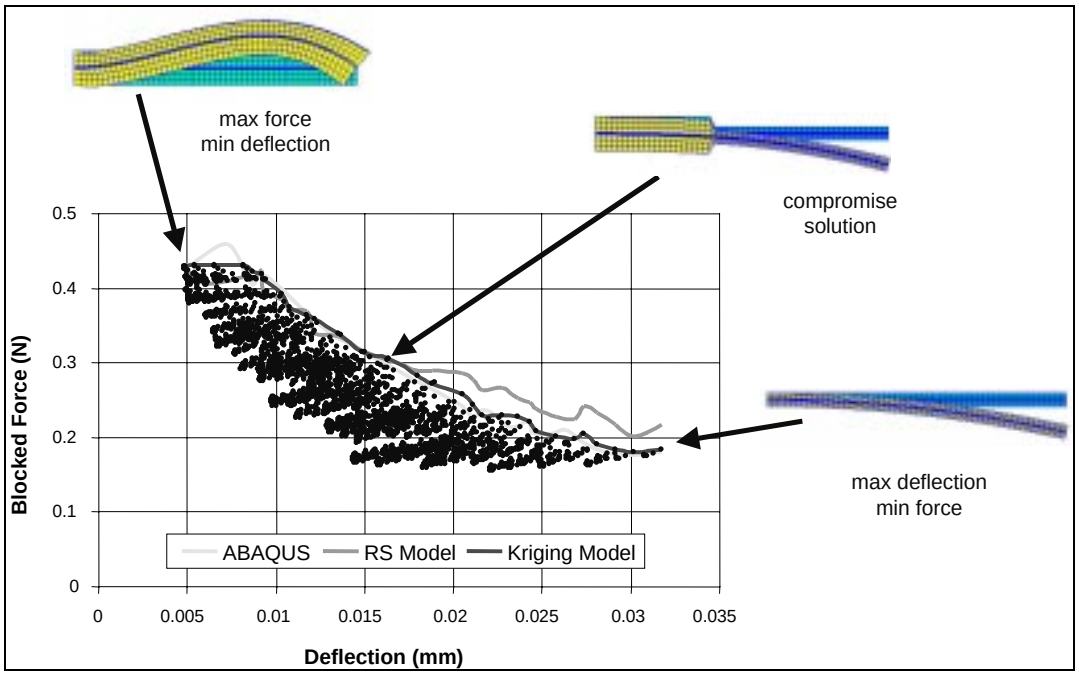

Figure 17 Pareto Frontiers Obtained Using Surrogate Approximations

Table 5 Effect of Weighting Factor on Solution using Response Surface Approximation

		Predicted		ABAQUS	
Weighting Factor, *w*	**Solution**	**δ (mm)**	**$F_{blocked}$ (N)**	**δ (mm)**	**$F_{blocked}$ (N)**
0.00 - 0.59		0.0318	0.2171	0.0317	0.1808
0.60 - 0.88	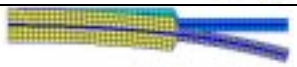	0.0096	0.4245	0.0092	0.4180
0.89 - 1.00	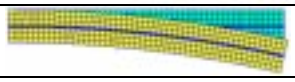	0.0052	0.4321	0.0048	0.4286

Table 6 Effect of Weighting Factor on Solution using Kriging Approximation

		Predicted		ABAQUS	
Weighting Factor, *w*	**Solution**	**δ (mm)**	**$F_{blocked}$ (N)**	**δ (mm)**	**$F_{blocked}$ (N)**
0.0-0.78		0.0317	0.1837	0.0317	0.1808
0.79		0.0143	0.2990	0.0148	0.3060
0.80-0.92	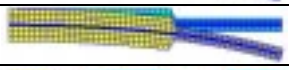	0.0092	0.4180	0.0092	0.4180
0.93-0.95		0.0082	0.4308	0.0082	0.3950
0.95-1.0		0.0048	0.4286	0.0048	0.4286